Sports Biomechanics
March 2009; 8(1): 60–77

Routledge
Taylor & Francis Group

A computational method for analysis of underwater dolphin kick hydrodynamics in human swimming

ALFRED VON LOEBBECKE[1], RAJAT MITTAL[1], RUSSELL MARK[2], & JAMES HAHN[3]

[1]*Department of Mechanical and Aerospace Engineering, George Washington University, Washington, DC,* [2]*USA Swimming, Colorado Springs, Colorado, and* [3]*Department of Computer Science, George Washington University, Washington, DC, USA*

(Received 31 March 2008; revised 29 May 2008; accepted 11 August 2008)

Abstract
We present a new method that combines the use of laser body scans, underwater video footage, software-based animation, and a fully unsteady computational fluid dynamics technique to simulate and examine the hydrodynamics of the dolphin kick. The focus of the current work is to model this particular stroke in all its complexity with minimal *ad-hoc* assumptions or simplifications. Simulations of one female and one male swimmer (both at about 1.7 m beneath the water surface) at velocities of 0.95 and 1.31 m/s and Strouhal numbers of 1.21 and 1.06 respectively are presented. Vorticity and fluid velocity profiles in the wake are examined in detail for both swimmers. A three-dimensional vortex ring is clearly identified in the wake for one of the cases and a two-dimensional slice through the ring corroborates previous experiments of Miwa et al. (2006). We also find that most of the thrust is produced by the feet and in both cases the down-kick produces much larger thrust than the up-kick.

Keywords: *Computational fluid dynamics, hydrodynamics, vortex rings, jet flow, kick asymmetry, active drag*

Introduction

As the name suggests, the dolphin kick resembles the sub-carangiform type of motion adopted by dolphins and other similar cetaceans (Lighthill, 1975), where the key feature is an undulatory wave motion that is initiated in the upper part of the body and which increases in amplitude as it propagates down towards the lower extremities (see Figure 1). In cetaceans, this mode of propulsion minimizes the displacement of the drag-producing forward parts of the body, and maximizes the displacement of the thrust-producing fluke.

In humans, the arms are outstretched and usually locked together in a streamlined position ahead of the head, and the body usually remains symmetric about the sagittal plane during the entire stroke. The swimmer may be oriented with their chest facing up, down or sideways depending on the particular stroke and individual preference. The displacement wave that travels the length of the body also has a small magnitude along the torso, and reaches a maximum at the toes. However, human anatomy constrains the smooth growth of this wave,

Correspondence: R. Mittal, Department of Mechanical and Aerospace Engineering, George Washington University, Suite T729, 801 22nd Street, Washington, DC 20052, USA. E-mail: mittalr@gmail.com

ISSN 1476-3141 print/ISSN 1752-6116 online
DOI: 10.1080/14763140802629982

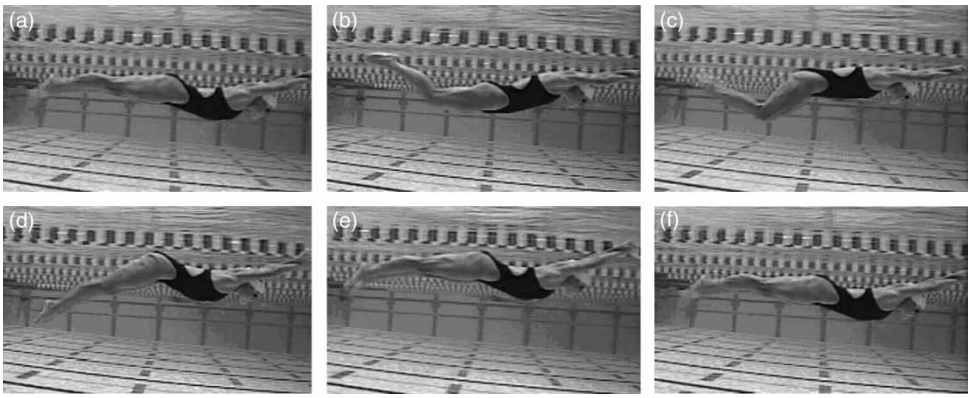

Figure 1. Six frames from a video of an Olympic-standard swimmer performing the dolphin kick.

as only three rotational joints – the hips, the knees, and the ankles – are available, as opposed to the many vertebrae that cetaceans possess. The asymmetry of the knee and ankle joints also leads to significant differences in the down-kick and the up-kick.

Two aspects of the dolphin kick make it a relatively easy stroke to model and study. First, the body undergoes a relatively simple motion during the stroke wherein it remains mostly symmetric about the sagittal plane. The arms do not exhibit any significant motion and the body of the swimmer does not roll about its long axis or pitch about the left–right axis. Thus, the kinematics of the dolphin kick are significantly simpler than, for instance, those of the front crawl, breaststroke or the backstroke. The stroke also occurs mostly at a significant distance (usually greater than 60 cm) below the water surface and, therefore, effects such as splashes, air-entrainment, and surface waves are not expected to have a significant impact on the hydrodynamics of this stroke.

Many previous experimental studies have investigated the active forces generated during swimming. For example, indirect methods such as the towing of participants (Clarys, 1978; Kolmogorov and Duplischcheva, 1992; Lyttle et al., 1999, 2000; Rennie et al., 1975; Toussaint et al., 2004) have been used. More direct methods, such as the MAD system (Hollander et al., 1986; Toussaint et al., 1988; Van der Vaart et al., 1987) or kinematic analysis (Berger et al., 1999; Payton and Bartlett, 1995), have also been used. However, all such experimental systems are limited by the fact that they tend to constrain the swimmer in one way or another and run the risk of altering the very features of the kinematics and hydrodynamics that are being studied. In this regard, computational fluid dynamics (CFD) offers a means of determining all the important quantities for a swimmer without altering the swimmer's natural gait. The CFD technique refers to the numerical simulations of the equations that govern the flow of fluids – that is, the Navier-Stokes equations on a computer (Tannehill et al., 1997). Computational fluid dynamics is a well-established tool in the engineering community but its use in swimming has been very limited to date. This is due to the fact that CFD simulations can in general require enormous amounts of computing time. This is particularly true in the case of swimming, since analysis of swimming requires one to include moving boundaries in the simulation and also resolve the flow around a complex-shaped, deforming object, all of which can further increase the complexity and the computational cost of the simulations.

Computational fluid dynamics was used for the first time in swimming by Bixler and Riewald (2002), who used it to study the drag/lift characteristics of the forearm. A more recent study involved a simulation of flow past a static swimmer in a streamlined position

(Bixler et al., 2007). Another recent study by Lyttle and Keys (2006) used commercial CFD software to perform quasi-steady simulations of the dolphin kick, breaking down the continuous cycle into a sequence of steady-state simulations. This approach, although interesting, has limitations for the analysis of swimming. The quasi-steady assumption can significantly modify the computed hydrodynamics and the computed forces on the body. Many of the mechanisms that are responsible for force generation during swimming are inherently unsteady in their origin. For example, added mass forces (Karamcheti, 1980), which are an important constituent of the total force, are proportional to the local body acceleration and this mechanism is essentially eliminated if a quasi-steady approach is adopted. Furthermore, the wake features produced in a quasi-steady simulation would also be significantly different from the realistic, fully unsteady case.

The purpose of the current study is to describe a new methodology for computational modelling and analysis of the hydrodynamics of swimming strokes. The methodology combines high-resolution laser scans of swimmers with animations and a high-fidelity, fully unsteady Navier-Stokes solver. The method is validated by computing the drag past a passive (streamlined) swimmer and making comparisons with previous studies. Subsequently, we focus on the dolphin kick and use two different models (one male and one female) to examine in detail the wake dynamics and thrust production mechanisms for this stroke. The results are intended to demonstrate that the approach developed here is capable of providing insights into swimming techniques that have hitherto been difficult to obtain via experiments or quasi-steady modelling techniques.

Methods

The key aspects of the methodology are (a) construction of an accurate geometrical model of a swimmer, (b) inclusion of realistic dolphin kick kinematics into the geometrical model (i.e. model animation), and (c) accurate, fully unsteady hydrodynamic simulations using this kinematically realistic model. We now describe the salient features of these three aspects.

Static geometrical model

Accurate, static geometrical models of swimmers were developed via three-dimensional laser body scans of one female and one male Olympic-standard athlete. Figure 2 shows the set-up of the laser scanning process and the resulting surface reconstruction of the athlete. The raw surface model obtained from the laser scan had to be modified to make it suitable for the CFD modelling. The software Rhino3D® (Becker and Golay, 1999) was used to separate the feet, which were originally joined together. This was necessary since video footage of swimmers performing the dolphin kick show that the feet may separate, sometimes markedly so, during the kick. The arms in the geometrical model were also connected with the head, which was a result of the body position adopted during the laser scans (see Figure 2). The arms were therefore also separated from the head. Both of these modifications required the creation of new surfaces to close or "patch" holes.

The resulting surface, which was in the form of the Initial Graphics Exchange Specification (IGES) file format, was then input into the software GAMBIT® (Fluent, Inc., 2005) and transformed into an unstructured surface mesh with triangular elements. A higher resolution (i.e. a more densely packed arrangement of smaller triangles) was used in regions of higher curvature. The final surface mesh consisted of 19,156 and 26,428 triangular elements for the female and the male model respectively.

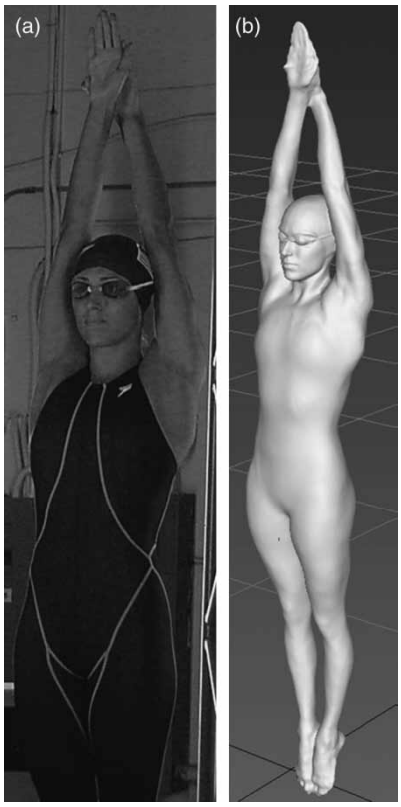

Figure 2. (a) Set-up during the laser-scanning process. (b) Surface reconstruction produced from laser scan.

Model animation

The next stage in the model development process was to instil the dolphin kick kinematics into the static geometrical model. Two elements are needed to accomplish this. The first is video footage from appropriate angle(s) of swimmers performing the dolphin kick, and the second is a methodology that allows us to animate the static model in a way that can match the video footage.

Video footage from underwater cameras located near the side walls of the swimming pool and which could translate horizontally with the swimmer was obtained for several Olympic-standard swimmers. Figure 1 shows a typical sequence of snapshots from such footage. As can be seen, issues such as bubble entrainment, resolution, and contrast can lead to loss of precision in these images. However, despite this, the images are mostly adequate for our purpose. In a typical dolphin kick, a sequence of 16–24 images over one representative dolphin kick cycle were extracted and the next step was to create an animated geometrical model that matched the swimmer in the images for the selected image sequence.

To bend/deform/articulate the static body in such a way as to match the video sequence, we used the software Autodesk MAYA® (Autodesk Maya Press, 2006). This software allowed us to include "joints" in the body so that the body could then be articulated with respect to these joints. The connectivity and properties of the joints result in a virtual "skeleton" that can be designed to produce many different types of articulation. Figure 3 shows two views of the joint structure (or "skeleton") that we incorporated into the model.

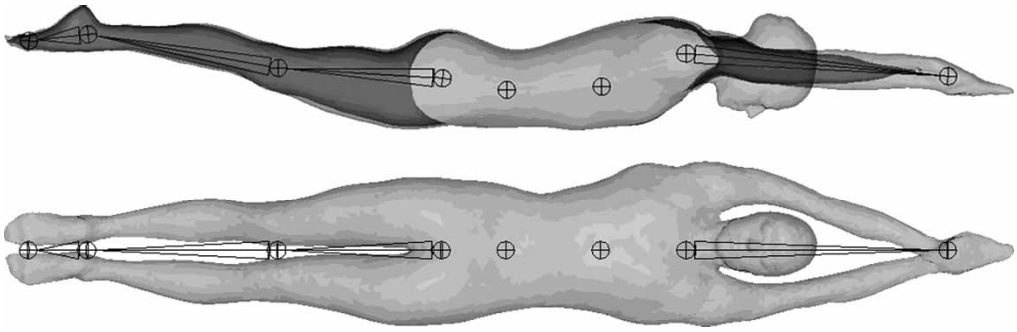

Figure 3. Side and top views of skeletal structure used in the model animation.

As can be seen, the joint structure attempts to mimic the major joints in the human body, including the wrist, shoulder, neck, vertebrae and hip, knee, and ankle joints. All joints are capable of rotation and translation. The joint at the shoulder and the joint at the hip represent so-called "root joints". They are at the top of their respective joint chain hierarchies and all lower-level joints move in accordance with them. The two root joints and the two unconnected joints in the torso allow for independent adjustment of the motion of the arms, the torso, and the legs. The influence of each joint upon the swimmer's body as well as the extent of the area affected by each joint is then adjusted individually. This is done so as to best reproduce the real swimmer's kinematics and also to ensure a smooth mesh and to avoid "wrinkling" in regions of high curvature and deformation.

Once the skeleton has been incorporated, each image is imported into MAYA and the static model deformed to match the swimmer's body configuration in the particular image (see Figure 4). The result of this process is a sequence of body surface grids that represent the body configuration at these instances. Although we manually matched only 16–24 phases in the dolphin kick over one cycle, the CFD simulations typically require that over 1000

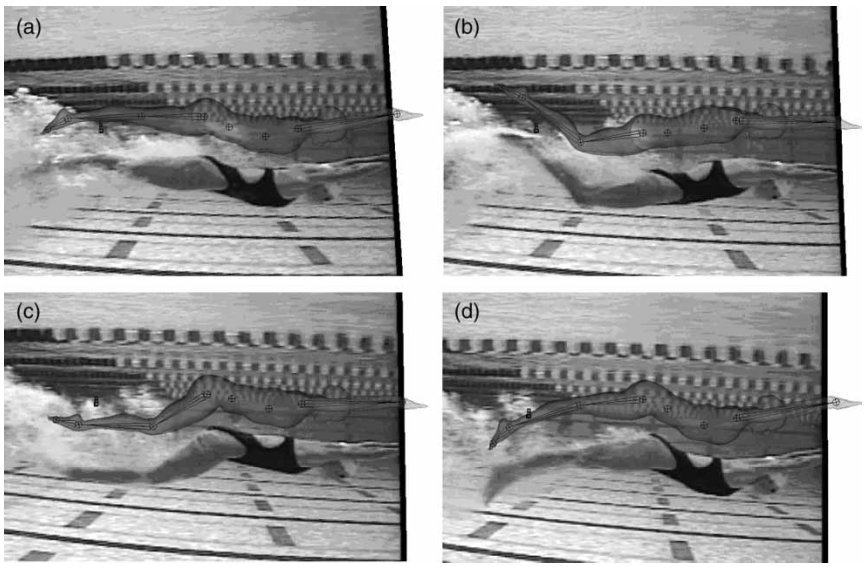

Figure 4. A sequence of four snapshots from the MAYA screen showing original video and matching geometrical model with joints

instances be available over each cycle. To produce these thousands of instances, we took the 16–24 extracted configurations and performed a spatio-temporal interpolation for the locations of the vertices of the surface triangles. This large sequence could then be concatenated with itself to produce a periodic multi-cycle simulation. As part of this interpolation process, we also obtained the velocity of the surface triangles at each of these phases and this information was used as a boundary condition in the CFD simulation.

Numerical method

The governing equations are the three-dimensional, fully unsteady incompressible Navier-Stokes equations for viscous flow with constant properties as follows:

$$\frac{\partial u_i}{\partial x_i} = 0 \tag{1}$$

$$\frac{\partial u_i}{\partial t} + \frac{\partial (u_i u_j)}{\partial x_i} = -\frac{1}{\rho}\frac{\partial p}{\partial x_i} + \nu \frac{\partial}{\partial x_i}\left(\quad \right) \tag{2}$$

where u_i are the velocity components, p is the pressure, ρ and ν are the fluid density and kinematic viscosity, and $i, j = 1, 2, 3$. The CFD software used in the current simulations is an in-house, immersed boundary solver (Mittal and Iaccarino, 2005) that is designed to solve flow past complex moving boundaries on stationary Cartesian grids. Further details regarding the numerical method can be found in Dong et al. (2006); here we provide a brief description of the key features of the method.

The Navier-Stokes equations (1–2) are discretized using a cell-centred, collocated, non-staggered arrangement of the variables (Tannehill et al., 1997). A second order QUICK scheme is used for spatial discretization (Tannehill et al., 1997). The equations are integrated in time using a fractional step method (Dong et al., 2006; Mittal et al., 2008). The immersed boundary method uses a ghost-cell formulation that is capable of handling arbitrarily complex two- and three-dimensional immersed stationary and moving boundaries (Mittal et al., 2008). It should be noted that unlike commercial solvers such as Fluent®, which can only model moving bodies in a quasi-steady manner, our solver solves the fully unsteady equations. This is a major departure from what has been done to date in CFD applications to swimming. The solver has been used recently to simulate the fluid dynamics associated with pectoral fin-based propulsion of fish (Mittal et al., 2006), where it has been shown to produce unsteady results that match well with accompanying experiments (Lauder et al., 2006).

The virtual swimmer is immersed in a rectangular computational domain for the purposes of the simulation. The set-up of the swimmer is designed to mimic swimming in a flume where the swimmer swims steadily and in place against a constant current. Uniform, unidirectional velocity boundary conditions are applied at all outside boundaries except at the downstream boundary, where an outflow condition is prescribed (Dong et al., 2006). On the body surface we apply the moving boundary velocity boundary conditions obtained from the spatio-temporal interpolation of the swimmer surface. Finally, Neumann boundary conditions are applied for the pressure at all outer boundaries and on the body surface.

The domain consists of a three-dimensional, non-uniform Cartesian mesh (Figure 5). Areas around the body and the near wake are provided with a higher resolution to resolve the boundary layers and vortex structures that are generated. The total number of mesh points

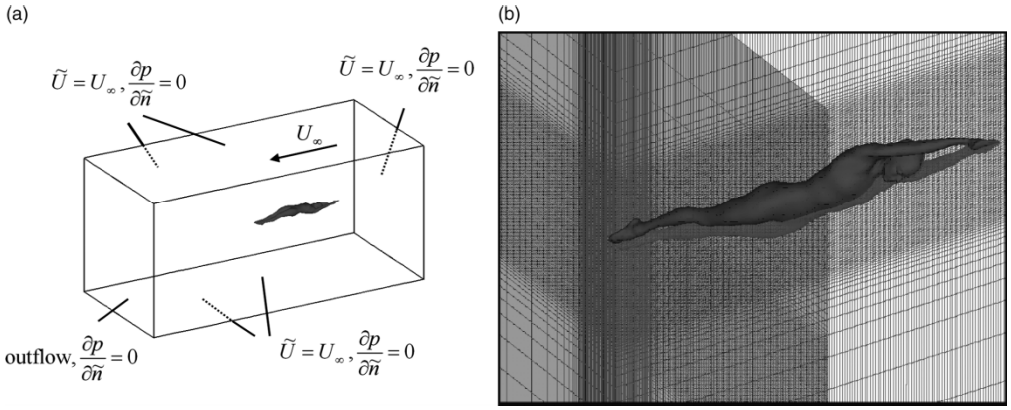

Figure 5. (a) Computational domain showing the inflow, outflow, and side boundaries together with the swimmer's body. (b) Close-up view of the grid near the body showing regions of enhanced resolution.

is limited by computational capacity. The current simulations have about 4.2 million mesh points. Furthermore, the simulations employ over 1000 time-steps per cycle providing high temporal accuracy. At each time step, the advancement of the flow equations takes full account of the boundary velocity and its acceleration through the boundary conditions. Thus, unlike the work of Lyttle and Keys (2006), no quasi-steady assumption is involved and we solved the flow with all the attendant unsteady effects. Simulations are run on a single processor of an in-house, 2.0-GHz AMD Opteron cluster and the simulations presented in the current paper took about 250 h of computer time per cycle on this computer. In a typical dolphin kick simulation, we simulated three cycles and only used the second and third cycles for our analysis to minimize the effect of initial transients on our results.

Passive drag and validation

The simulations of the swimmers performing the dolphin kick are preceded by a computational analysis of a static swimmer in a streamlined position. In this analysis, flow past a female swimmer in the position shown in Figure 6(a) at a speed of 1.0 m/s is simulated. The passive drag from this simulation provides a baseline for comparison of active drag in the

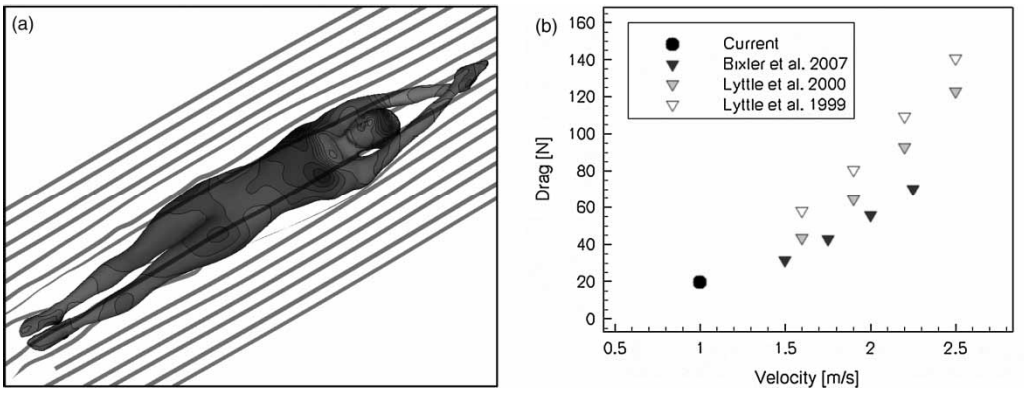

Figure 6. Results of simulations past a static, streamlined body. (a) Streamline pattern and surface pressure distribution. (b) Comparison of current passive drag results with existing data.

dolphin kick cases. The computed drag is also compared with other available data to provide some level of validation for the current solver.

Strouhal number, thrust, and streamwise momentum

A key non-dimensional parameter in animal swimming is the Strouhal number, which is defined as $St = fA/V$, where f is the kick frequency, A is the total toe amplitude of the kick, and V is the swimmer's average speed. The Strouhal number is a key determining factor for both the thrust and the power efficiency of swimming in fish and cetaceans (Rohr and Fish, 2004). It is now fairly well established that most efficient swimming in animals occurs at a Strouhal number ranging from 0.2 to about 0.4 and that most of these marine animals generally swim in this range of Strouhal numbers.

The thrust generated by the swimmer was one of the key quantities of interest in the current study. As will be shown here, CFD not only allows us to compute this quantity, it also allows a level of analysis regarding this quantity that can shed additional insight into swimming techniques and their correlation with thrust production. In the current simulations, the force on the swimmer was directly computed by integrating the computed pressure and shear stress on the body.

We were also interested in the excess streamwise momentum in the wake of the swimmer executing the dolphin kick. This quantity is estimated as $(U^2 - V^2)$, where U is the time and spanwise averaged streamwise velocity of the flow at a particular location and V is the average speed of the swimmer. Regions where this quantity is positive correspond to addition of momentum to the flow, whereas regions where this quantity is negative correspond to removal of momentum from the fluid. Newton's Third Law implies that momentum imparted by the body onto the fluid in the streamwise direction produces an equal and opposite (thrust) force on the body.

Results and discussion

Here we describe the results from our simulations of the two models of dolphin kick included in the current study. We also use the results to provide some insights into the hydrodynamics of the dolphin kick. However, before the description of the dolphin kick simulations, we present some results of the passive drag validation study.

Passive drag

We simulated flow past a female swimmer in a static, streamlined position at a speed of 1.0 m/s (Figure 6a). The passive drag for this case is computed to be 19.7 N and this is compared with available measurements/estimates in Figure 6(b). Lyttle et al. (1999) conducted prone, streamlined glide towing measurements of humans at a depth of 0.6 m below the water surface with the towing velocity ranging from 1.6 to 3.1 m/s. Lyttle et al. (2000) towed swimmers at a depth of 0.5 m below the water's surface at five different speed increments from 1.6 to 3.1 m/s. Five different positions were used, namely prone and lateral streamlined glide, prone freestyle kick, and prone and lateral dolphin kick. The prone streamlined glide position was considered to be most similar to our passive swimmer, and therefore those results were used as a comparison. Bixler et al. (2007) conducted simulations using the Fluent CFD code of a swimmer in streamlined glide at a depth of 0.75 m at velocities ranging from 1.5 to 2.25 m/s. These prone streamlined glide simulations were also considered to be apt comparisons for our current results. The results from the current

simulation are very much inline with these previous results and validate the fidelity of the modelling procedure employed here. It should be noted that in our simulation, the shear force constituted ~6 N or ~30% of the total drag, with the remainder due to pressure, which is also in line with previous studies (Bixler et al., 2007).

Dolphin kick

The parameters velocity (V), body length from fingertips of the outstretched arms to the toes (L), overall surface area (S), kick-amplitude (A), kick frequency (f), Strouhal number (St), and mean active drag for both cases are shown in Table I. For the current swimmers, the Strouhal numbers are 1.21 and 1.06, which are higher than the value for most efficient swimming. This is not unexpected for two reasons. First, humans have not evolved for efficient swimming and, second, swimming efficiency is not necessarily important for short-distance events. In fact, swimming at high Strouhal numbers is usually associated with high thrust and low efficiency (Fish, 2004), which is appropriate for fast swimming over short distances.

Flow features

The dynamics of any complex unsteady viscous flow are best described in terms of the vortex structures produced in the flows (Dong et al., 2006). Here we show a sequence of vortex structure topologies generated by the swimmers over one kick. The vortex structures are shown in terms of one isosurface of the imaginary part of the complex part of the eigenvalues of the velocity gradient tensor. This quantity has been used before to detect vortex structures quite successfully for a variety of complex flows, including the vortex structures produced by swimming fish (Mittal et al., 2006). The rows of images in Figures 7 (female) and 8 (male) represent, from top to bottom, the time instances of 0.2, 0.4, 0.6, 0.8, and 1.0 of the cycle period τ. Three-dimensional vortex structures, a two-dimensional sagittal slice of flow vectors and flow speed contours, and a sagittal slice of vorticity contours are shown from left to right at each of the five instants in time. In the slice of vorticity contours, solid contour lines indicate counterclockwise rotation and dotted lines indicate clockwise rotation. For the female case, the down-kick starts at 0.28 τ, the up-kick starts at 0.72 τ; for the male case, the down-kick starts at 0.24 τ and the up-kick starts at 0.76 τ.

A number of common features can be observed at all these stages. First, almost all the vorticity shed by the body during the stroke is produced from regions below the knee. These are obviously the parts of the body that are undergoing the largest magnitude of motion. Some small vortex structures are shed from the head and hips but, for the most part, the areas of the body above the knee shed very little vorticity. This indicates that the flow in these regions of the body is nearly fully attached. The most dominant feature in the wake is a convoluted vortex ring that is shed at the end of the extensive stroke. In contrast, the up-kick produces only a cluster of smaller vortices with no distinct topology and these dissipate quite rapidly leaving only a pair of thin vortices.

Table I. Dolphin kick kinematic parameters and mean active drag.

	V (m/s)	L (m)	S (m^2)	A (m)	f (1/s)	St	Mean active drag (N)
Female	0.95	2.30	1.63	0.64	1.8	1.21	134.7
Male	1.31	2.80	2.15	0.58	2.4	1.06	251.7

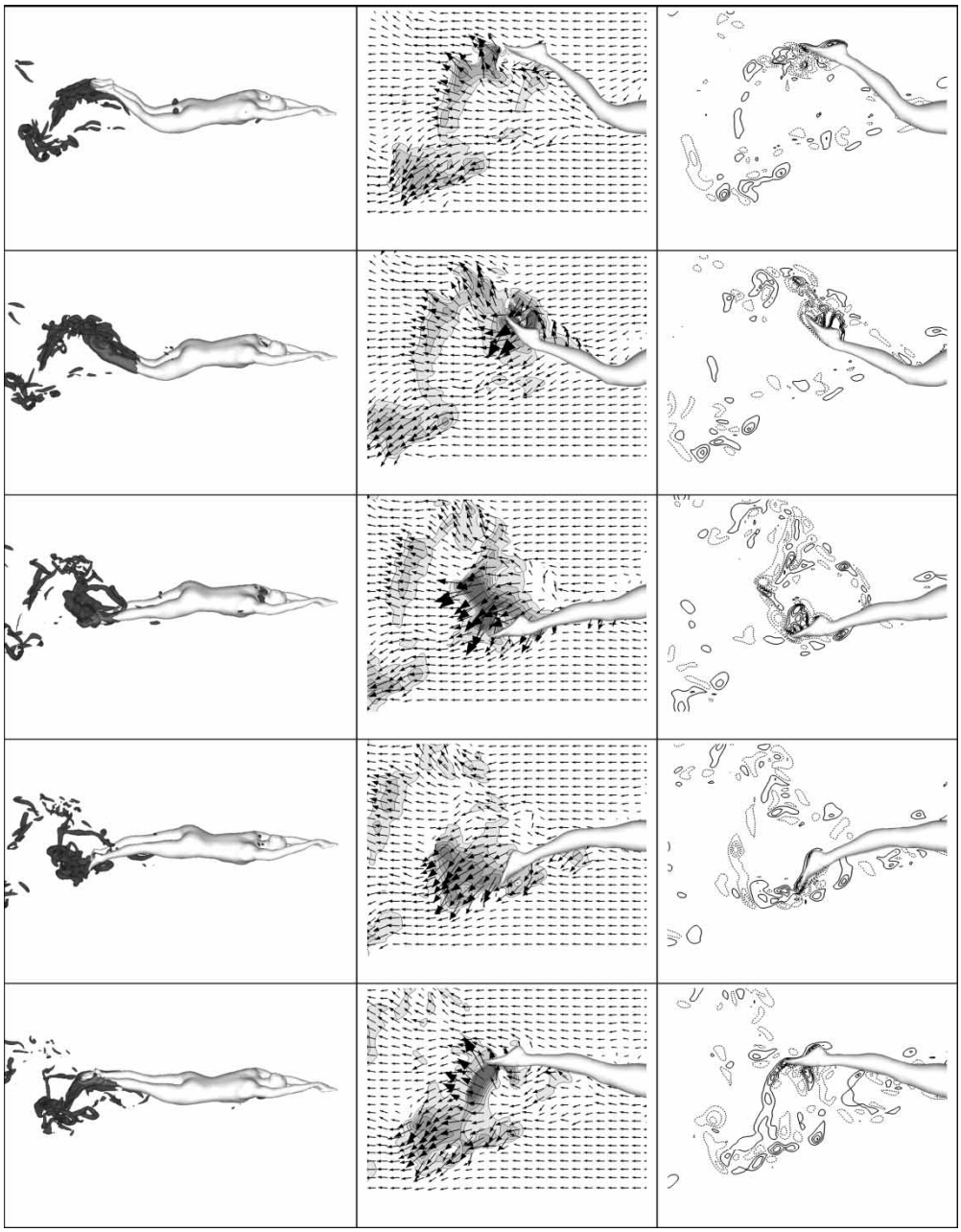

Figure 7. For the female case, from top to bottom, rows of images at 0.2, 0.4, 0.6, 0.8, and 1.0 of cycle period τ. From left to right: topology of vortex structures, a slice containing flow vectors and flow speed contours, and a slice containing vorticity contours (solid lines represent counterclockwise rotation, dotted lines represent clockwise rotation).

Figure 9 is a series of images taken of the male swimmer at time 0.88 τ, shortly after the start of the up-kick. As before, vortex structures, flow vectors, flow speed contours, and vorticity contours are shown. At this time the structure created by the down-kick has convected slightly downstream of the feet. A three-dimensional vortex ring can be clearly

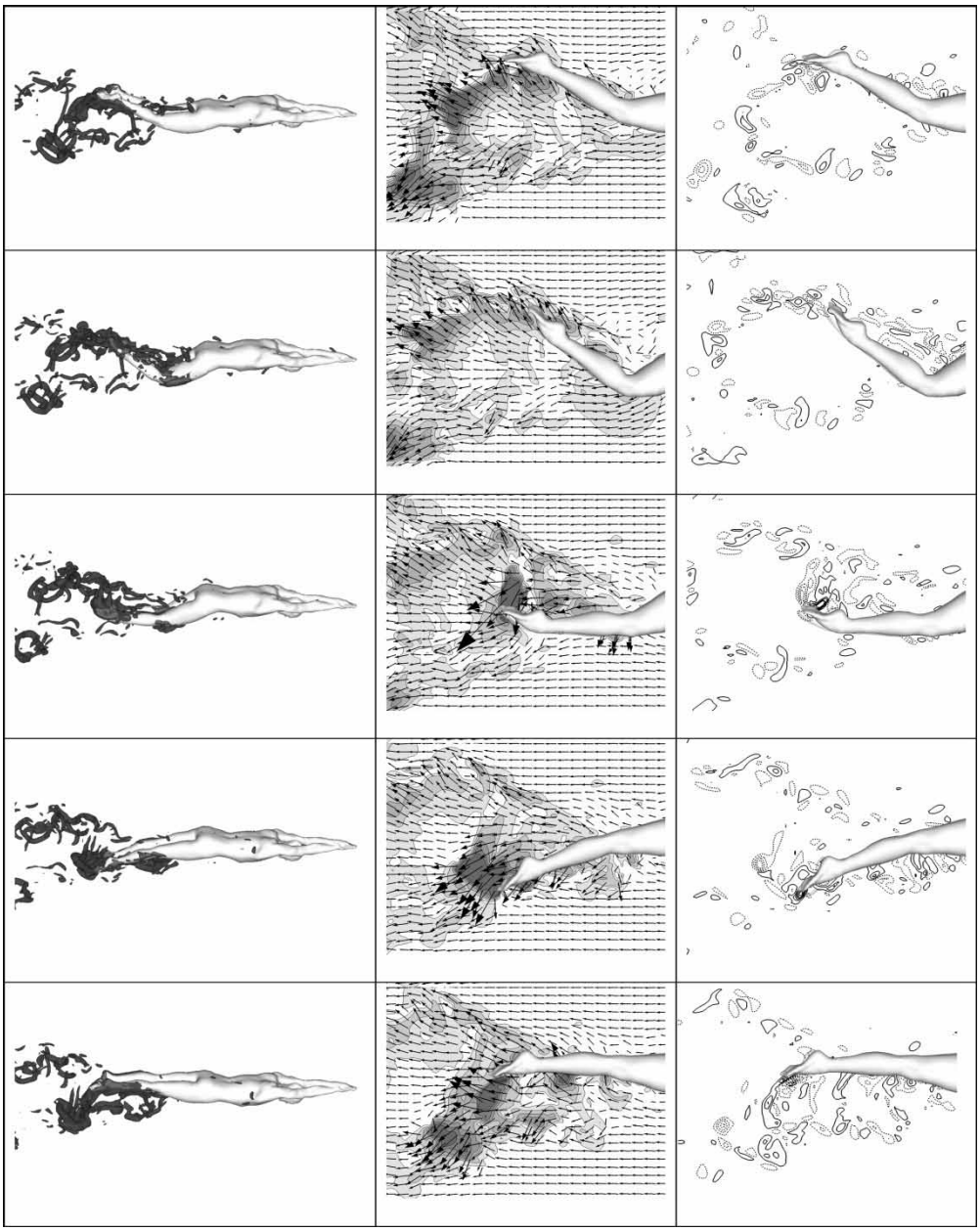

Figure 8. For the male case, from top to bottom, rows of images at 0.2, 0.4, 0.6, 0.8, and 1.0 of cycle period τ. From left to right: topology of vortex structures, a slice containing flow vectors and flow speed contours, and a slice containing vorticity contours (solid lines represent counterclockwise rotation, dotted lines represent clockwise rotation).

seen. The appearance of this vortex ring at the end of the extensive kick has significant implications for the hydrodynamics. A stationary vortex ring produced in a fluid will move due to self-induction and can also induce a highly directed jet. Vortex rings also persist for relatively long durations without much change in shape, and this coupled with the self-induced motion also implies that vortex rings are optimally suitable topologies for creating

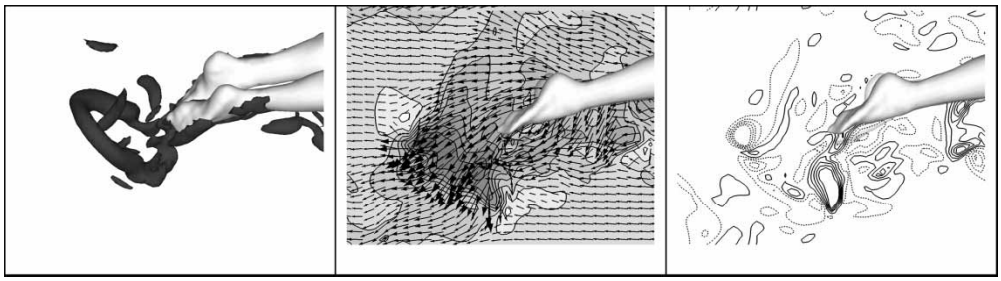

Figure 9. For the male case, from top to bottom, topology of vortex structures, slice containing velocity vectors and velocity contours, and slice containing vorticity contours (solid lines represent counterclockwise rotation, dotted lines represent clockwise rotation) at 0.88 of cycle period τ.

thrust. This is borne out in nature where it is found that a wide variety of swimming animals that are highly adapted for aquatic propulsion can and do produce vortex ring wakes as they propel themselves in water (Dabiri et al., 2005; Drucker and Lauder, 2001; Marten et al., 1996; Mueller et al., 2001).

The formation of vortex rings during the fly-kick is a phenomenon that is not unknown in the competitive swimming arena. Colwin (2002) describes what he terms the "fling-ring", which essentially refers to the vortex ring structure found in the current simulation. This can be confirmed in the second image of Figure 9, which shows the flow velocity in the core of the vortex structure. It can be seen that the vortex ring produces a distinct, high-velocity jet. The third image in Figure 9 clearly shows two counter-rotating vortices accompanying the jet. These vortices are the sectional part of the three-dimensional vortex ring, as suggested by Miwa et al. (2006). Figure 10 shows a sequence of snapshots from a video of an Olympic-standard swimmer performing the dolphin kick. A clearly distinct and compact vortex structure (identified by entrained bubbles) is shown to be released at the end of the extensive kick in a manner very similar to that seen in the simulations. Arellano et al. (2002) have also identified similar vortex rings in their experiments. Interestingly, the wake structure seen here is also similar to that observed for eels by Tytell and Lauder (2004), who noted strong lateral jets separated by vortices of similar orientation in the wake.

Figure 11 shows the profile of the excess streamwise momentum in the wake of the swimmer executing the dolphin kick. The plot indicates the formation of an intense and compact jet in the wake centred at about $Y = 2.4$. This is precisely the region where the vortex ring from the extensive kick is released into the wake. This further confirms that the extensive portion of the kick is responsible for most of the thrust production. Furthermore, the plot also confirms the connection between the vortex ring topology and thrust production, and this is discussed further in the following section.

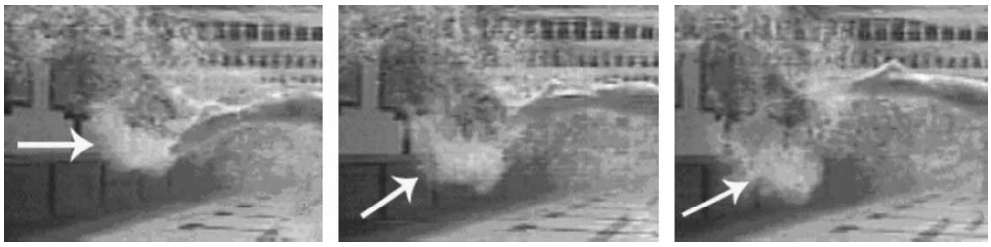

Figure 10. Images from video footage of the dolphin kick. Entrained bubbles help visualize the flow. The white arrows have been added to help indicate the vortex ring structure shedding off of the feet.

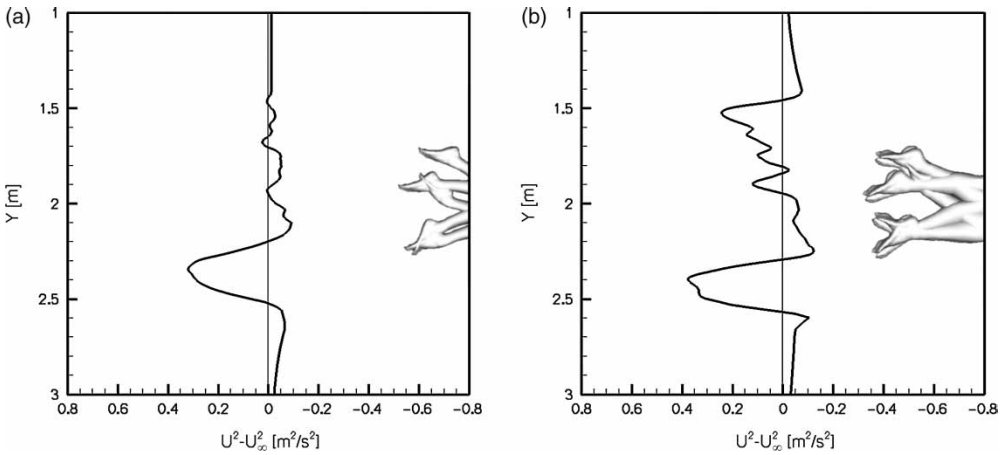

Figure 11. Time- and span-averaged momentum deficit/excess in swimmer's wake for (a) the female case and (b) the male case.

Thrust generation

Figure 12 shows the variation of the net streamwise force on the swimmer over one dolphin kick cycle. Negative values indicate drag and positive values indicate thrust. Point A indicates the start of the down-kick and point B indicates the start of the up-kick. It can be seen that the shear forces are small, nearly steady, and exclusively drag-producing. We note that for both (a) the female case and (b) the male case there are two clearly identifiable thrust peaks. For the female case, two drag peaks, which are similar in magnitude, occur around the phase when the foot is either at the top-most or bottom-most point in its trajectory. For both cases, the thrust peaks occur after the foot reverses direction, whereas the drag peaks occur before reversal of direction. In contrast to the drag peaks, one of the thrust peaks is much larger than the other. This large thrust occurs during the extensive part of the kick, whereas the smaller thrust peak occurs during the up-kick. Thus, there is significant asymmetry in the forces produced during the two portions of the kick. This is a clear manifestation of the anatomical asymmetry in human anatomy that comes to bear during these segments of the kick. Whereas in the extensive kick, extension at the knee couples with plantar flexion at the ankle to produce a smoother wave-like motion, the same is not true during the up-kick. It is also

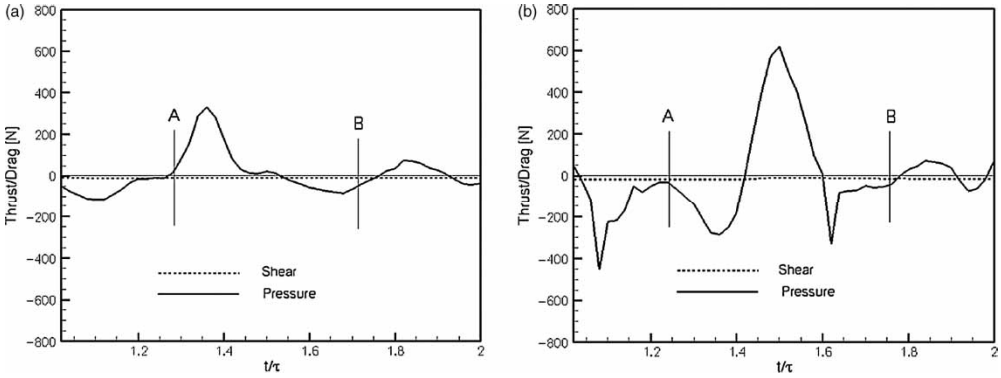

Figure 12. Time variation of net streamwise force over one cycle for (a) the female case and (b) the male case. Point A marks the start of the down-kick and point B marks the start of the up-kick.

important to note that the higher thrust coincides with the production of the vortex ring described in the previous section, thereby confirming the importance of vortex ring formation. The aforementioned kick asymmetry was also noted by Jensen and McIlwain (1979). They determined that the down-kick produced thrust and that the up-kick actually produced drag. Videler and Kamermans (1985) also studied the dolphin kick in actual dolphins and found strikingly similar results. They found the dolphins accelerated during the down stroke and decelerated during the up stroke. They also found that the propulsive forces of the down stroke were larger than those of the up stroke.

The CFD results can be probed further to gain additional insights into thrust production and swimmer performance. For instance, the concept of "active drag", which refers to the drag produced by the body during swimming, has received much attention in the swimming community (see, for example, Clarys, 1978; Huijing et al., 1988; Kolmogorov and Duplishcheva, 1992; Toussaint and Truijens, 2005; Toussaint et al., 2004). Since for steady swimming thrust has to balance out this active drag, it has been posited that a good swimming stroke is one that limits active drag, thereby requiring the least amount of thrust. However, since for steady swimming the net average force on the body is necessarily zero, it becomes very difficult to measure active drag experimentally. This is especially true for the dolphin kick, where an active drag measurement system such as MAD (Toussaint et al., 2004) cannot be used. Computational fluid dynamics, however, provides a unique opportunity to examine the issue of active drag.

As pointed out earlier, the body surface of the swimmer is made up of triangular elements and it is possible to compute the hydrodynamic force on each triangular element individually. To compute the active drag for the swimmer at any instant in time, we sum the forces from all the triangles that exhibit a force in the streamwise (drag) direction. Similarly, all the triangles that exhibit a force opposite to the flow direction allow us to compute the instantaneous propulsive force. It should be noted that although at any given instant these two force components can have different magnitudes, their time-averaged values should be nearly equal and opposite during steady swimming.

Figure 13 shows the variation of these forces for the two swimmers. It should be noted that the shear forces are less than 4% of the mean active drag (female case) but comparable to the passive shear drag. Pressure forces therefore dominate the active force. First, as anticipated, the propulsive force shows significant variation over the cycle with a large peak

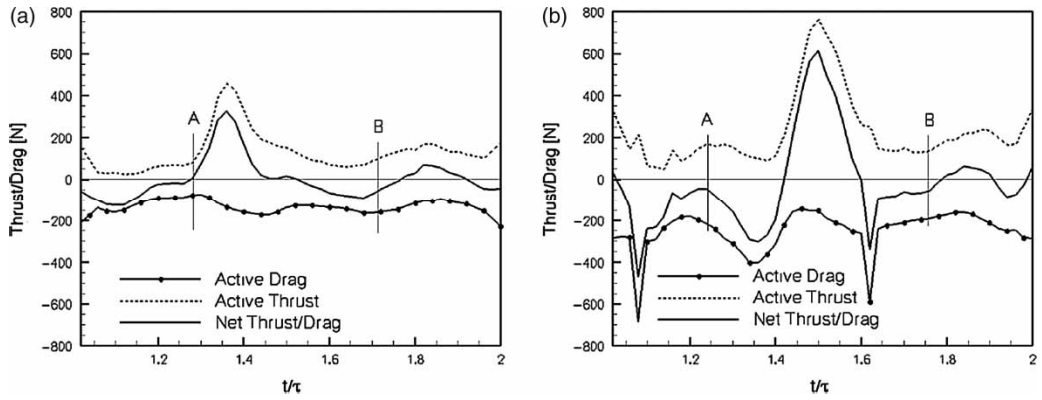

Figure 13. Time variation of active drag and thrust produced by the swimmer during the dolphin kick for (a) the female case and (b) the male case. Point A marks the start of the down-kick and point B marks the start of the up-kick.

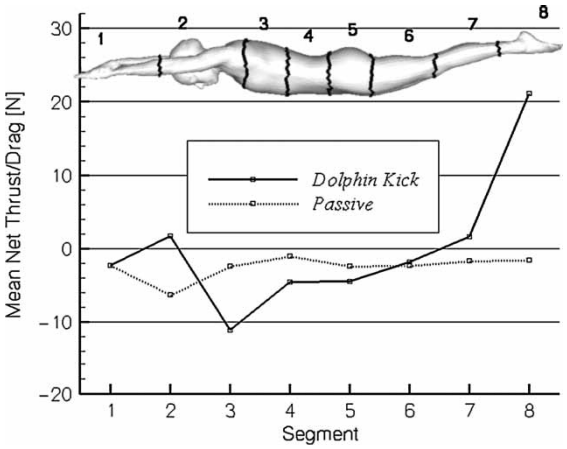

Figure 14. Mean streamwise active and passive force by segment for the female case.

corresponding to the extensive part of the kick. Second, even the drag force shows some temporal variation over the cycle. The computed dimensional value of mean active drag force for the female and male swimmer is 134.7 and 251.7 N respectively. Thus, the active drag during the dolphin kick is significantly larger than the passive drag. Past measurement of active drag has been conducted for the front crawl stroke and typical measured values were about 82.26 N at a mean velocity of 1.51 m/s (Toussaint et al., 1988). Thus the current values are significantly higher. Clearly, the higher than expected values of active drag could partly be a result of modelling uncertainty. However, there is some literature that suggests that such high values might not be outside the norm. For instance, Van Tilborgh et al. (1987) used velocity fluctuations to estimate thrust forces in breaststroke swimming and recorded values of up to 348 N in one case with a mean velocity of 1.14 m/s. Thus, active drag is very much stroke dependent and would be expected to be very different for the front-crawl, the breaststroke, and the dolphin kick. Nevertheless, validation of the current results against experimental measurements would be highly desirable.

Next, we determine which segments of the body are responsible for thrust production and which are responsible for drag production. This is important, since this is the first step in connecting swimming performance with technique. We focus here on the female swimmer and divide the swimmer's body into eight segments, as shown in Figure 14. The mean streamwise force coefficient for each segment is then computed and again shown in Figure 14. The figure also includes force coefficients from the aforementioned passive case. As expected in the passive case, all segments produce only drag. In the active case, the last segment (segment 8) produces most of the thrust. Thus, the simulations indicate that the feet are responsible for most of the thrust production and that other parts of the leg do not contribute directly to propulsion.

Conclusions

In this paper, we have described a novel effort to accurately model the hydrodynamics of a swimming stroke using fully unsteady computational fluid dynamics modelling. The methodology developed couples laser scans and underwater video footage with grid generation and animation software to develop a highly accurate geometric representation

of a swimmer executing the dolphin kick. This geometrical model is then inserted into CFD software that allows us to simulate flow past complex moving bodies on stationary Cartesian grids. The solver employed is fully unsteady and this is important in so far as it is known that unsteady effects are a key component of thrust production in swimming animals.

This computational methodology is used to simulate two cases of Olympic-standard swimmers executing the dolphin kick. One key finding of the current study is the formation of a distinct vortex ring type structure during the extensive portion of the dolphin kick. We also found that most of the propulsive force is produced during the extensive portion of the kick whereas the up-kick produces significantly less propulsive force. The asymmetry of the stroke is also evident in the momentum change in the wake and is a manifestation of the anterior–posterior joint asymmetry in the human body. We also compared the computed active drag with the passive drag and found that not only is the active drag significantly higher than the passive drag, it also varies over the stroke. By computing the forces produced by the various segments of the body, we find that most of the active drag during the dolphin kick is produced by the chest, abdomen, and hips, whereas most of the propulsive force is produced by a small portion of the legs extending from just above the ankle to the toes. Thus, a focus on foot motion and ankle flexibility could have a large impact on dolphin kick performance.

The current paper was intended to demonstrate the viability of fully unsteady CFD-based modelling for the analysis of swimming hydrodynamics. Experimental analysis of swimming is confounded by a number of issues, including the need to work with humans and the inherent difficulty of extracting forces and wake information without in some way altering the natural gait of the swimmer. In this regard, the CFD-based method presented here is promising and we expect that it will be able to complement existing experimental efforts and lead to a better understanding of swimming hydrodynamics.

References

Arellano, R., Pardillo, S., and Gavilán, A. (2002). Underwater undulatory swimming: Kinematic characteristics, vortex generation, and application during the start, turn, and swimming strokes. In *XXth International Symposium on Biomechanics in Sports – Applied Program – Swimming*. Cáceres, Spain: Universidad de Extremadura.

Autodesk Maya Press (2006). *Learning Autodesk Maya 8*. Berkeley, CA: Sybex Inc.

Becker, M., and Golay, P. (1999). *Rhino NURBS 3D Modeling*. Indianapolis, IN: New Riders Publishing.

Berger, M. A. M., Hollander, A. P., and De Groot, G. (1999). Determining propulsive force in front crawl swimming: A comparison of two methods. *Journal of Sports Sciences*, *17*, 97–105.

Bixler, B., Pease, D., and Fairhurst, F. (2007). The accuracy of computational fluid dynamics analysis of the passive drag of a male swimmer. *Sports Biomechanics*, *6*, 81–98.

Bixler, B., and Riewald, S. (2002). Analysis of a swimmer's hand and arm in steady flow conditions using computational fluid dynamics. *Journal of Biomechanics*, *35*, 713–717.

Clarys, J. P. (1978). Relationship of human body form to passive and active hydrodynamic drag. In E. Asmussen, and K. Jorgensen (Eds.), *Biomechanics VI-B* (pp. 120–125). Baltimore, MD: University Park Press.

Colwin, C. (2002). *Breakthrough swimming*. Champaign, IL: Human Kinetics.

Dabiri, J. O., Colin, S. P., Costello, J. H., and Gharib, M. (2005). Flow patterns generated by oblate medusan jellyfish: Field measurements and laboratory analyses. *Journal of Experimental Biology*, *208*, 1257–1265.

Dong, H., Mittal, R., and Najjar, F. M. (2006). Wake topology and hydrodynamic performance of low-aspect-ratio flapping foils. *Journal of Fluid Mechanics*, *556*, 309–343.

Drucker, E. G., and Lauder, G. V. (2001). Locomotor function of the dorsal fin in teleost fishes: Experimental analysis of wake forces in sunfish. *Journal of Experimental Biology*, *204*, 2943–2958.

Fish, F. E. (2004). Strouhal numbers and optimization of swimming by odontocete cetaceans. *Journal of Experimental Biology*, *207*, 1633–1642.

Fluent, Inc. (2005). *FLUENT 6.2 user's guide*. Lebanon, NH: Fluent, Inc.

Hollander, A. P., De Groot, G., Van Ingen Schenau, G. J., Toussaint, H. M., De Best, H., Peeters, W. et al. (1986). Measurement of active drag during crawl arm stroke swimming. *Journal of Sports Sciences*, *4*, 21–30.

Huijing, P. A., Toussaint, H. M., Mackay, R., Vervoorn, K., Clarys, J. P., de Groot, G. et al. (1988). Active drag related to body dimensions. In B. E. Ungerechts, K. Wilke, and K. Reischle (Eds.), *Swimming science V* (pp. 31–37). Champaign, IL: Human Kinetics.

Jensen, R. K., and McIlwain, J. (1979). Modeling of lower extremity forces in the dolphin kick. In J. Terauds, and E. W. Bedingfield (Eds.), *International series of sport sciences, vol. 8: Swimming III* (pp. 137–147). Baltimore, MD: University Park Press.

Karamcheti, K. (1980). *Principles of ideal-fluid aerodynamics*. Malabar, FL: Robert Krieger.

Kolmogorov, S. V., and Duplishcheva, O. A. (1992). Active drag, useful mechanical power output and hydrodynamic force coefficient in different swimming strokes at maximal velocity. *Journal of Biomechanics*, *25*, 311–318.

Lauder, G. V., Madden, P., Mittal, R., Dong, H., and Bozkurttas, M. (2006). Locomotion with flexible propulsors: I. Experimental analysis of pectoral fin swimming in sunfish. *Bioinspiration and Biomimetics: Learning from Nature*, *1*, S25–S34.

Lighthill, J. (1975). *Mathematical biofluid dynamics*. Philadelphia, PA: Society for Industrial and Applied Mathematics.

Lyttle, A. D., Blanksby, B. A., Elliott, B. C., and Lloyd, D. G. (2000). Net forces during tethered simulation of underwater streamlined gliding and kicking techniques of the freestyle turn. *Journal of Sports Sciences*, *18*, 801–807.

Lyttle, A. D., Elliot, B. C., Blanksby, B. A., and Lloyd, D. G. (1999). An instrument for quantifying the hydrodynamic drag of swimmers – a technical note. *Journal of Human Movement Studies*, *37*, 261–270.

Lyttle, A. D., and Keys, M. (2006). The application of computational fluid dynamics for technique prescription in underwater kicking. *Revista Portuguesa de Ciências do Desporto*, *6* (suppl. 2), 233–255.

Marten, K., Shariff, K., Psarakos, S., and White, D. (1996). Ring bubbles of dolphins. *Scientific American*, *275*, 83–87.

Mittal, R., Dong, H., Bozkurttas, M., Lauder, G. V., and Madden, P. (2006). Locomotion with flexible propulsors: II. Computational modeling of pectoral fin swimming in sunfish. *Bioinspiration and Biomimetics: Learning from Nature*, *1*, S35–S41.

Mittal, R., Dong, H., Bozkurttas, M., Najjar, F. M., Vargas, A., and Von Loebbecke, A. (2008). A versatile sharp interface immersed boundary method for incompressible flows with complex boundaries. *Journal of Computational Physics*, *27*, 4825–4852.

Mittal, R., and Iaccarino, G. (2005). Immersed boundary methods. *Annual Review of Fluid Mechanics*, *37*, 239–261.

Miwa, T., Matsuuchi, K., Shintani, H., Kamata, E., and Nomura, T. (2006). Unsteady flow measurement of dolphin kicking wake in sagittal plane using 2C-PIV. In J. P. Vilas-Boas, F. Alves, and A. Marques (Eds.), Biomechanics and medicine in swimming X: Book of abstracts. *Portuguese Journal of Sport Sciences*, *6* (suppl. 1), 64–66.

Mueller, U. K., Smit, J., Stamhuis, E. J., and Videler, J. J. (2001). How the body contributes to the wake in undulatory fish swimming: Flow fields of a swimming eel (*Anguilla anguilla*). *Journal of Experimental Biology*, *204*, 2751–2762.

Payton, C. J., and Bartlett, R. M. (1995). Estimating propulsive forces in swimming from three-dimensional kinematic data. *Journal of Sports Sciences*, *13*, 447–454.

Rennie, D. W., Pendergast, D. R., and Di Prampero, P. E. (1975). Energetics of swimming in man. In J. P. Clarys, and L. Lewillie (Eds.), *Swimming II* (pp. 97–104). Baltimore, MD: University Park Press.

Rohr, J. J., and Fish, F. E. (2004). Strouhal numbers and optimization of swimming by odontocete cetaceans. *Journal of Experimental Biology*, *207*, 1633–1642.

Tannehill, J. C., Anderson, D. A., and Pletcher, R. H. (1997). *Computational fluid mechanics and heat transfer*. London: Taylor & Francis.

Toussaint, H. M., Beelen, A., Rodenburg, A., Sargeant, A. J., De Groot, G., Hollander, A. P. et al. (1988). Propelling efficiency of front-crawl swimming. *Journal of Applied Physiology*, *65*, 2506–2512.

Toussaint, H. M., Roos, P. E., and Kolmogorov, S. V. (2004). The determination of drag in front crawl swimming. *Journal of Biomechanics*, *37*, 1655–1663.

Toussaint, H. M., and Truijens, M. (2005). Biomechanical aspects of peak performance in human swimming. *Animal Biology*, *55*, 17–40.

Tytell, E. D., and Lauder, G. V. (2004). The hydrodynamics of eel swimming: I. Wake structure. *Journal of Experimental Biology*, *207*, 1825–1841.

Van der Vaart, A. J. M., Savelberg, H. H. C. M., De Groot, G., Hollander, A. P., Toussaint, H. M., and Van Ingen Schenau, G. J. (1987). An estimation of drag in front crawl swimming. *Journal of Biomechanics*, *20*, 543–546.

Van Tilborgh, L. M., Stijnen, V. V., and Persyn, U. J. (1987). Using velocity fluctuations for estimating resistance and propulsion forces in breaststroke swimming. In B. Jonsson (Ed.), *Biomechanics X* (pp. 779–784). Champaign, IL: Human Kinetics.

Videler, J., and Kamermans, P. (1985). Difference between upstroke and downstroke in swimming dolphins. *Journal of Experimental Biology*, *119*, 265–274.